Delft University of Technology

Faculty of Mechanical, Maritime and Materials Engineering

MSc Thesis

Measuring Ground Reaction forces in Running Specific Prostheses

A Fibre Optical Sensor approach

By

Tijmen Jan Pieter Seignette

Supervisors:
Prof. dr. F.C.T. van der Helm
Dr.ir. O.K. Bergsma

August 18, 2021

Abstract

Running Specific Prosthesis (RSP) allow amputee sprinters to compare to the best able-bodied sprinters in the world. In RSP research, the current state of the art mainly focusses on highly detailed analysis of discrete moments in the sprint, but more data of the entire sprint process in terms of RSP characteristics and sprinting technique are needed for further development of RSP-design and sprinting technique. In recent research Petrone et al. [4] and Galvão et al. [2] developed instrumented RSPs for collection of Ground Reaction Force (GRF)s suring sprinting, however both methods have disadvantages for implementation of instrumented RSPs in amputee sprinting training purposes. A different instrumented RSP approach was taken in this research by measuring surface strain in Fiber Bragg Grating (FBG) sensors attached to two RSPs; one Ottobock 1E90 and one Gyromotics ArcX Sport. From the collected data the internal moments and axial forces could be approximated, from which the GRF magnitude, direction and point of application were determined. The sensor system was calibrated in a 1-DOF load-cell compression bench and was conducted to a field test in which a participant performed load shifting, walking and running trails on the instrumented Gyromotics RSP. The compression tests showed that the measurement system complied to design requirements and that it was possible to estimate the point of application of the GRF. The field test indicated that loads applied in different directions than applied in the compression bench could lead to measurement errors. Additional calibration, predominantly in the x-direction, is therefore needed.

Acknowlegdements

This project has been shaped by the involvement of many people from different disciplines. This thesis would not certainly not have been possible without the guidance of my supervisors, Prof. Dr. F.C.T. van der Helm and Dr. Ir. O.K. Bergsma. I would like to thank Prof. Dr. F.C.T. van der Helm for his encouraging words whenever I got stuck and his valuable feedback moments. I would like to thank Dr.Ir. O.K. Bergsma for his contagious enthusiasm for the project and for sharing his practical approach in problem solving.

I would also like to thank Ir. Ewoud Velu from the PhotonFirst company for his efforts guiding me though the world of optical sensors and for lending me the needed equipment for the project. Whenever I had questions about the working principles, practical implementation or application of optical sensors I could always knock on his door.

Dave Ruitenbeek and Alexander Uithof have both helped me a lot in preparing, setting up and analysing the compression testing at DASML, all with a healthy dose of humor.

I would like to thank Guido Hendriks from Gyromotics for his inspiration, his insights in the world of running prosthetics and for letting me participate in the development of their prosthesis and letting me use the end product for my project.

Lastly but certainly not least, I would like to thank Pinar Ates, Ivo Schouten and Frank Jol for participating in this project.

Contents

List of Figures iv

List of Tables vi

Abbreviations vii

1 Introduction 1

2 Methodology 2
2.1 Sensor system design requirements 2
2.2 Reference frames and definitions 3
2.3 Initial calculations 4
2.4 Sensor layout and spectral design 4
2.5 Compression tests 6
2.6 Field tests 7

3 Results 9
3.1 Expected strains in system 9
3.2 Variance in system 9
3.3 Static calibration through compression tests 10
3.4 Field tests 12

4 Discussion 17

5 Conclusions 19

References 20

A Appendix A - Spectral design, sensor layout 21

B Appendix B - FEA results 23

C Appendix C - Raw Polarization data 24

D Appendix D - Raw compression test data 26

E Appendix E - Raw field test data 29
E.1 Jogging trails - short l_{step} 29
E.2 Jogging trails - regular l_{step} 29
E.3 Jogging trails - long l_{step} 30

F Appendix F - Inverse calculation model 34

G Appendix G 38

H Appendix G 42

List of Figures

1 Reference frames and definitions . . . 3
2 FEA schematic overview . . . 4
3 Axial force and bending force calculation method . . . 5
4 Instrumented RSPs: (a) shows the Ottobock 1E90 prototype, (b) shows the Gyromotics ArcX Sport . . . 6
5 Experimental setup in compression bench. . . . 7
6 Field test setup of the FBG measurement system . . . 8
7 Calibration of GRF for the Gyromotics ArcX Sport . . . 11
8 Calculated GRF point of application, distance from sensor 1 . . . 11
9 Measured GRFy during repeated compression test - Gyromotics ArcX Sport. . . . 12
10 Measurement error of the FBG computed GRFy compared to the Zwick force . . . 13
11 The computed GRF in the first weight shift trail. . . . 13
12 GRF profiles of walking trails . . . 15
13 GRF profiles of jogging trails . . . 16
14 GRFy calculated from strain in field test - jogging, regular l_{step} - trail 1. 17
15 Sensor Locations on the Gyromotics ArcX Sport . . . 21
16 Sensor layout instrumented Ottobock 1E90 . . . 22
17 Sensor layout instrumented Gyromotics ArcX Sport . . . 22
18 FEA results Ottobock 1E90 . . . 23
19 FEA results Gyromotics ArcX Sport . . . 23
20 Unperturbed sensor data, f_s = 1,928 kHz. . . . 24
21 Polarization sensor data, f_s = 1,928 kHz. . . . 24
22 FFT of raw sensor signals . . . 25
23 Raw strain data - Ottobock 1E90 . . . 26
24 Calibrated GRF curve Ottobock 1E90 . . . 27
25 GRF Point of application - Ottobock 1E90 . . . 27
26 Raw strain data - Gyromotics ArcX Sport . . . 28
27 Normal probability plot for the measured error (difference in Zwick force and GRFy computed through FBG sensors) in several compression tests. These plots indicate that the used calibration method . . 28
28 Jogging short l_{step} - trail 1. Individual lines represent the steps of the entire trail. . . . 29
29 Jogging short l_{step} - trail 2. Individual lines represent the steps of the entire trail. . . . 29
30 Jogging short l_{step} - trail 3. Individual lines represent the steps of the entire trail. . . . 30
31 Jogging regular l_{step} - trail 1. Individual lines represent the steps of the entire trail. . . . 30
32 Jogging regular l_{step} - trail 2. Individual lines represent the steps of the entire trail. . . . 31
33 Jogging regular l_{step} - trail 3. Individual lines represent the steps of the entire trail. . . . 31
34 Jogging long l_{step} - trail 1. Individual lines represent the steps of the entire trail. . . . 32

35 Jogging long l_{step} - trail 2. Individual lines represent the steps of the entire trail. 32
36 Jogging long l_{step} - trail 3. Individual lines represent the steps of the entire trail. 33

List of Tables

1 Maximum calculated and measured surface strains on sensor locations - Ottobock 1E90 9
2 Maximum calculated and measured surface strains on sensor locations - ArcX Sport 9
3 FBG variance and polarization 10
4 Instrumented Gyromotics ArcX specifications 18

Abbreviations

f_s	Sampling frequency.
CFRP	Carbon Fibre Reinforced Polymer.
FBG	Fiber Bragg Grating.
FEA	Finite Element Analysis.
FOS	Fiber Optical Sensing.
GRF	Ground Reaction Force.
IMU	Internal Measurement Unit.
RSP	Running Specific Prosthesis.

1 Introduction

Track sprinting is one of the spectacular sports disciplines in the Paralympics and similar to the Olympic track sprinting events, the Paralympic events have their own sports stars. Not only the athletic side of the sport is more professional than ever but the same can be said for the equipment used in Paralympic disciplines.

In the case of a below-the-knee amputation (T62 and T64 classes) most track sprinting athletes use a Running Specific Prosthesis (RSP). The world records in these classes come very close to able-bodied sprinter times in the track sprinting disciplines[3]; at the time of writing the most recent 100-meter world record 10.54 seconds by Johannes Floors - the best time of able bodied sprinters is 9.58 seconds by Usain Bolt.

Although RSPs appear to be a simple design, the combination of human body-prosthetic interaction, the Carbon Fibre Reinforced Polymer (CFRP) material properties and the non-intuitive dynamic behaviour of the shape of the RSP make for complex design parameters. The development of innovative RSP designs is therefor dependent on extensive data-collection and analysis.

An analysis was done of the state-of-the-art in RSP data collection and RSP characterization. Four characterization methods were distinguished; Finite Element Analysis (FEA) modelling, static or dynamic lab testing, Digital Image Correlation methods, and force plate analyses.

Except for two studies found in literature every characterization method involved either one specific static or dynamic load type or a detailed biomechanic analysis. Although extensive analysis is possible with the methods, only one RSP orientation or one discrete moment in the sprint can be analysed. These methods therefor lack the flexibility of collecting in-field over entire sprints.

A different approach was taken by Petrone et al. [4] and by Galvão et al. [2]. Both methods involved an instrumented prosthesis that measures the strain at certain locations on the prosthesis' material from which the GRFs are deducted. The major advantage of this instrumented RSP method is that it allows for in-field measurements throughout an entire sprint and comparing the different phases in the sprint. These measurements could therefore yield important data for RSP development or sprinting technique training.

Petrone et al. made use of strain gauge bridges mounted on three geometrically defined positions. The measured strain is converted to an internal moment from which the GRFs are determined. Next to a calibration in both x-direction and y-direction a field test with athletes was conducted. This method uses a low amount of sensors, but yields results that are comparable to force platform measurements and are therefore very useful for the mentioned purposes of data collection. However, minimizing the weight and bulk of the total sensor system including receivers could be an issue as well as the (long term) fragility of the system as it is applied on the material surface.

The method proposed by Galvão involves the use of Fiber Bragg Grating (FBG) sensors. These sensors detect the strain in an optical fibre in which they are written. The approach by Galvão makes use of 17 of these FBG sensors. The optical fibre in which these sensors are written is then embedded in the CFRP laminate of the RSP. This measurement system is calibrated by directly correlating the measured strains in the FBGs to the applied force in a compression bench. For validation

a participant also walked with the prosthesis, but no direct comparison with force-plate data was conducted. The advantage of using an embedded FBG sensor system as done by Galvão is that fragility is minimized. If mounted correctly, the connector end where the optical fibre exits the prosthesis laminate, is the only fragile point of the instrumented RSP. The downside of the approach taken by Galvão is that it is expensive to manufacture due to the large number of sensors needed.

In order to create a mobile instrumented RSP that could be used in a similar manner to a regular RSP but with the added possibility of measuring GRFs, a combination of both approaches has to be taken. The robustness of embedded FBGs and the physical interpretation of the strain which results in flexibility of the approach by Petrone seem like a good starting point for a new iteration of an instrumented RSP design.

The research goal of this thesis is therefore formulated as:

> *"Develop and validate a measurement system prototype using Fibre Optical Sensors that is able to detect the Ground Reaction Force magnitude, direction and point of application on a Running Specific Prosthesis when being used."*

This research goal leads to the following research questions:

- What is the suitability of optical sensing in determining the ground reaction forces in running specific prostheses?
  - What are the measurement system specifications (sensitivity, accuracy, precision) and how do these compare to the required measurement system specifications?
  - What are the advantages and disadvantages of the sensor system compared to previously researched characterization methods?

2 Methodology

2.1 Sensor system design requirements

To evaluate the measurement system prototype two sets of design specifications were formulated: a set of performance requirements and a set of physical requirements.

The performance requirements are formulated as:

- The system should be able to detect the horizontal and vertical force components of the GRF.
- The system should be able to detect the point of application of the GRF.
- The sensor system should have a measurement error (variance and bias) of lower than 5 % of the maximum GRF in x-direction and y-direction.
- The sampling rate of the system should be at least $1kHz$ as contact times of 0,2 s are expected [7] and to account for adequate data analysis possibilities.
- The application of the sensor system should not alter the mechanical characteristics of the RSP.

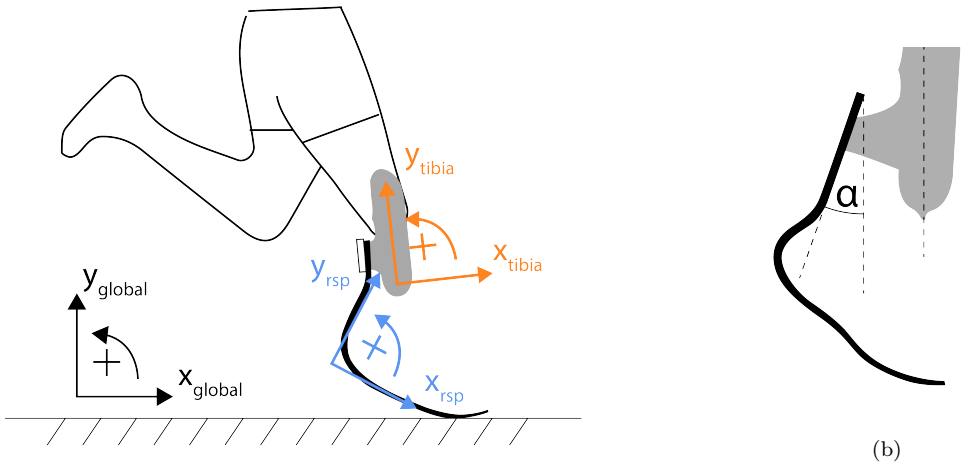

(a) (b)

Figure 1: Reference frames as chosen in the research setup. The RSP reference frame (a) is chosen such that the axial direction of the FBGs in bridges 1 and 2 (FBG 1, FBG 2, FBG 5 and FBG 6 in figure 3) is aligned with the x-axis. The tibia reference frame is chosen such that the construction line of the head of the fibula to the valve of the prosthesis socket is aligned with the y-axis of the tibia reference frame. In (b) can be seen how angle α, the alignment angle, determines the orientation of the RSP with respect to the tibia. α is the angle between the straight proximal part of the prosthesis and y-axis of the tibia reference frame y_{tibia}.

And the physical requirements are formulated as:

- The weight of the measurement system added to the RSP should not exceed 0.100 kg.
- The sensor system should not impair the gait of the athlete.
- External device size of the sensor system should not exceed the following measurements: 200 mm x 300 mm x 300 mm.

2.2 Reference frames and definitions

For this research, the calculations on the GRFs are viewed as a 2D, sagittal plane problem. First a set of reference frames in this plane is introduced to allow for the expression of the calculated GRF in both the global reference frame and the local reference frame (in which the x-axis aligns with the neutral line through both sensor pairs). These reference frames are shown in figure 1a.

Not only the orientation of the tibia defines the RSP orientation with respect to the global reference frame; also the mounting angle α has to be considered. The definition of α can be found in figure 1b. For the initial calculations, the FEA and the compression tests, multiple alignment angles α will be considered.

The forces used as an input for the initial calculations (inverse calculation model and FEA) were derived from research by Weyand et al. [6]. These forces in Weyands study are normalised for bodyweight of a sprinter. An athlete of 70kg was considered during this research. For running at 10 m/s, the vertical GRF peak is 3.24 times body weight, and the horizontal GRF is -0.51 times body weight.

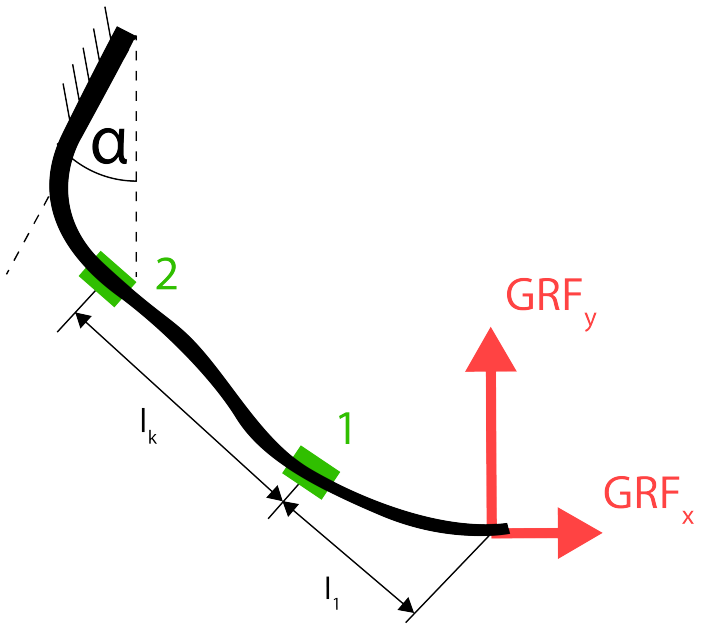

Figure 2: FEA schematic overview. The proximal end of the RSP, which would normally be fixed to the stump, is fixed in the FEA model. The angle φ defined the orientation of the prosthesis with respect to the global reference frame.

2.3 Initial calculations

Two different RSP models were considered for instrumentation: one Ottobock 1E90 RSP and a Gyromotics ArcX Sport blade. Prior to determining the sensor layout on the prostheses an estimation of the strain distribution and strain magnitudes was done. Using both an inverse calculation model in Matlab and a FEA (Autodesk Fusion 360) strain estimations were made. For the inverse calculation model the proximal end of the RSP was considered fixed. For the FEA the situation as shown in figure 2 was used. The Matlab model for the inverse calculations can be found in appendix F.

2.4 Sensor layout and spectral design

It was chosen to calculate the GRF based on the the internal forces and moments calculated from the strain at chosen locations on the top and bottom of the prosthesis (see figure 15 for the Ottobock sensor layout, and figure 3 for the Gyromotics ArcX Sport sensor layout).

The sensor layout was designed with two major criteria in mind: (1) maximal decoupling of the forces in x- and y-direction and (2) highest strain magnitude while conforming to (1). Using the maximum strain found by the inverse calculation model and the FEA a sensor layout and accompanied spectral design for the FBGs was designed.

The sensor locations were chosen such that angle between the the axial directions of the FBG 1, 2, 5 and 6 (FBG 1, 2, 3 and 4 for the Ottobock 1E90 prototype) in the xy-plane of the RSP-reference frame (see figure 3) is minimized. The strains are split in an axial strain component and a bending strain component on each sensor

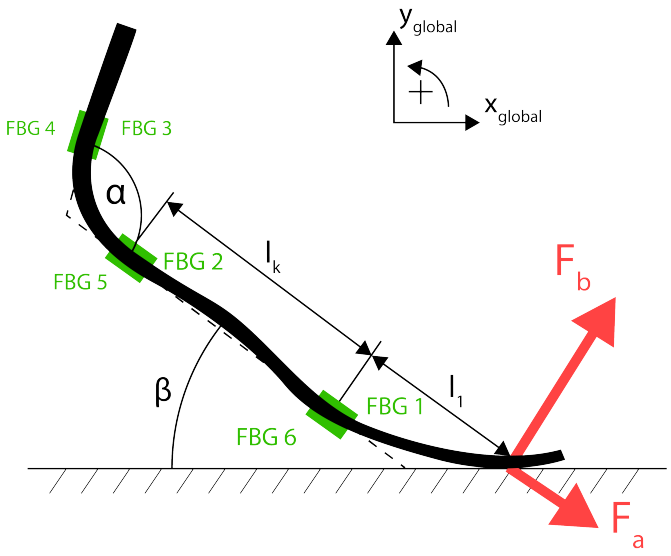

Figure 3: Schematic drawing of the FBG placement on the prosthesis. Using the axial and bending strain components measured in the FBGs, F_a and F_b, the GRF components at the point of application in the RSP reference frame can be calculated. Also the location of the point of application, l_1 can be determined from the calculations.

bridge location. Using the RSP geometry at the bridge location location axial force in every sensor bridge section is calculated, from which the GRF contributions in the RSP reference frame are calculated:

$$F_b = \frac{(M_2 - M_1)}{l_k} \tag{1}$$

$$l_1 = \frac{M_1}{F_b} \tag{2}$$

Also the point of application of the GRF with respect to the sensor locations, l_1, can be approximated. Using the experimentally retrieved angle β (see section 2.5) the forces measured in the local reference frame could be expressed in the global reference frame.

It was chosen to multiplex all FBGs in series so that a single channel Fiber Optical Sensing (FOS) interrogator could be used to read out the FBGs. This meant that the sensor spacing in the wavelength domain should have ample room for the calculated strains found by the inverse model and the FEA.

In the spectral design there was accounted for the direction and magnitude of both F_b and F_a. Throughout the contact phase of the step, sensors 1, 2 and 3 would mainly be subjected to a negative strain and sensors 4, 5, and 6 would mainly be subjected positive strain. The spectral design was chosen such that all sensors could be detected simultaneously while ensuring that the FBG wavelengths did not interfere with each other. The chosen wavelengths for the sensors can be found in figures 16 and 17 in appendix A.

(a) (b)

Figure 4: Instrumented RSPs: (a) shows the Ottobock 1E90 prototype, (b) shows the Gyromotics ArcX Sport

2.4.1 Prototype production

Two RSPs were instrumented with FBGs: one Ottobock 1E90 prosthesis and one Gyromotics ArcX Sport prosthesis. FBGS Femtosecond polyamide-coated FBG sensors were glued to the prosthesis surface in the chosen locations. Dymax OP24-REV-6 adhesive was used for the FBG ends of the fibres, and the more elastic Norland Optical 61 adhesive was used for each FBG section of the fibre to minimize stick-slip effects at the fibre-adhesive interface. For the first prototype, the Ottobock 1E90, the sensors were connected in series by means of FC-APC connectors. In the second prototype, the Gyromotics ArcX Sport, the FBGs were spliced in series at the appropriate length so that slack fibre was minimized. The sensors were connected to a PhotonFirst Gator interrogator. Using PhotonFirst Gator Operating Software (Version 3.0) the data was retrieved and processed.

2.5 Compression tests

Both prostheses were subjected to a static load compression test using a ZWICK-/ROELL 250 kN tensile/compression bench for calibration. The compression bench was equipped with strain sensors at the top clamp which allows for detecting forces in y-direction of the global reference frame. By means of `Correlated solutions VIC 3D` software, the angle β was approximated at each load. Also the calibration settings for the FBG interrogator software were determined during these compression tests.

The proximal end of the RSP was fixed in the upper clamp such that both translation and rotation were constraint in order to replicate the fixture of the RSP to a socket. The distal end of the RSP was constraint in the y-direction by means of a cart which only moves in the x-direction (see figure 5).

Since the RSP is fixed in the compression bench several angles α have to be considered for calibration. These angles result in a different working line of the force through the RSP which therefore alters the moment arm and thus the deformation of the material. α was determined at 35°, 40° for the Ottobock 1E90, for the Gyromotics ArcX Sport α was determined at 27°, 32°, and 37°. These angles were based on the recommended socket mounting angles provided by the manufacturers. The GRF_{max} used in the compression tests was set equal to the maximal force mentioned

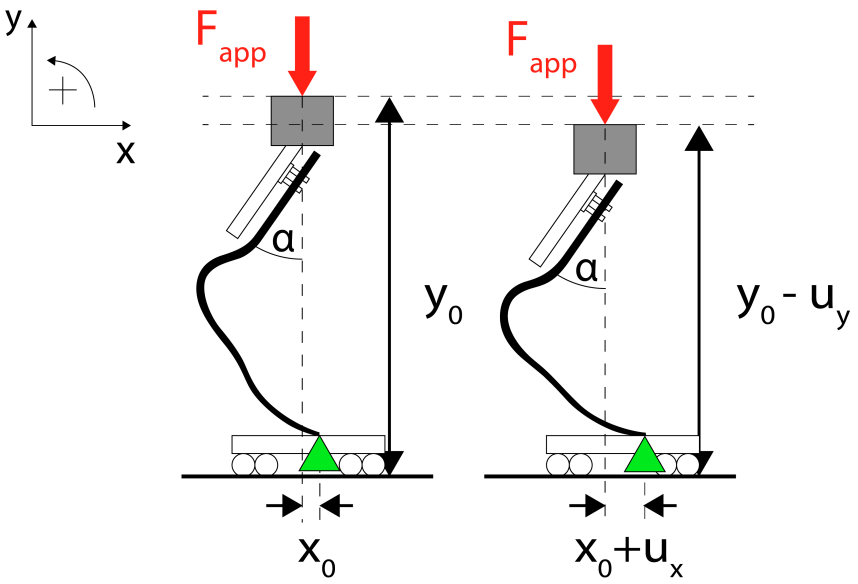

Figure 5: Experimental setup in the compression bench. The application of a vertical displacement of the top clamp induces a deformation of the RSP shape. Due to the geometry and the directional stiffness the height in the y-direction will change, but also the displacement of the distal end will alter with $x_o + u_x$.Therefore not only a resultant force in x and y-direction in the distal end of the RSP will appear but also a resultant moment in the clamped end of the RSP can be expected.

in section 2.2 which were also used in the inverse model and FEA computations.

Three separate tests are conducted:

- Steady increase of the force from 0 N to GRF_{max} with a force plateau of 5 seconds at GRF_{max} after which the force is reduced to 0 N.
- A cyclic test in which test 1 is repeated 4 times on end.
- A step test where the froce is increased from 0 N to GRF_{max} with intervals every 250 N and a plateau at GRF_{max}, after which the reverse is done at intervals of 250 N until 0 N is reached.

2.5.1 Calibration of the sensor system

In order to calibrate the sensor system an optimization procedure was used in MATLAB (see appendix G). The internal force and moment calculations in the computational model were parameterized. Using the least-square error function of the measured GRF compared to the Zwick measurement, the optimization function `fmincon` was used to yield the calibration parameters for the sensor system.

2.6 Field tests

The field tests took place on an artificial turf field at the Frank Jol B.V. company situated at the Friendship Sports Center. Only the ArcX Sport blade was used for these field tests. The experimental setup used in the field test is shown in figure 6.

Internal Measurement Unit (IMU) sensors (Shimmer 3) were attached to the

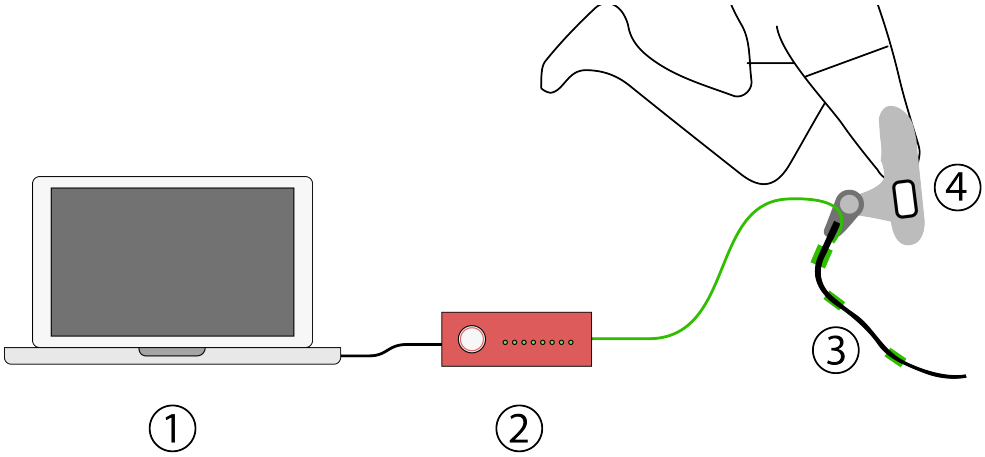

Figure 6: Test setup of the field tests. The laptop (1) is connected to the FBG interrogator (2) (PhotonFirst Gator). The instrumented Gyromotics ArcX Sport prosthesis (3) is connected to the interrogator via a patch cable. The IMU (4) (Shimmer 3) is used to record the orientation of the stump relative to the global reference frame.

socket with the IMU y-axis corresponding to y_{tibia}. These sensors described the position and orientation of the socket and the RSP in terms of the global reference frame. IMU data was recorded at 51,2 Hz. For the field test analysis the computed angle about all all three axes of the blade-reference frame was used as an input for the FBG data analysis. To compensate for gyroscopic drift the angles were computed by combining the acceleromter data and gyroscope data. The FBG data was recorded at 19,8 kHz. The Matlab model for analysis can be found in appendix H

The participant, an unilateral, transtibial amputee athlete (length 1.70 m, weight 65 kg) was asked to perform 3 activities in 3 variants of which each variant was repeated 3 times. Before every trail, the participant was asked to do a knee rise with the RSP-mounted leg. This indicated a cue point for synchronisation of the IMU data and FBG data. The walking and running took place on a 15-meter course on the artificial turf field. The participant was asked to do:

- cyclic load shift between two legs
  - low frequency
  - medium frequency
  - high frequency
- walking (approximately 1.5 m/s)
  - short step length
  - medium step length
  - high step length
- running (approximately 4 m/s)
  - short step length

- medium step length
- high step length

Also a null-measurement was done before and directly after the activities described above in order to find possible effects of sensor drift in the FBGs.

3 Results

3.1 Expected strains in system

The results for the inverse calculation model and the FEA can be found in tables 1 and 2. These are the strains found in location 1 and 2 at the angle α for which the maximum strains occurred. For the Ottobock 1E90 $\alpha = 35°$ gave the largest strain, for the Gyromotics ArcX Sport $\alpha = 27°$ gave the largest strain. For reference the FBG measured strains of the compression tests with the same angles α are included.

For both the FEA model and the inverse MATLAB model the calculated strain at strain bridge 1 was lower than at strain bridge 2. The MATLAB model estimates the strains to be lower at the sensor locations in both the Ottobock 1E90 model (9,3% lower for location 1 and 15,5% lower for location 2) and the Gyromotics ArcX Sport (8,5% lower for location 1 and 32,6% lower for location 2).

The FBG measured maximal strains for location 2 showed to be similar to the predicted strains (3,22% higher than the FEA predicted strain of the Ottobock 1E90, 0,96% lower than the FEA predicted strain of the Gyromotics ArcX Sport). On location 1 for the Ottobock 1E90 the FBG measured strain was 49,6% higher than the FEA predicted strain, whereas the FBG measured strain for the Gyromotics ArcX Sport on location 1 was 34,1% lower than the FEA predicted strain.

	$\mu\varepsilon_1$	% of FEA strain	$\mu\varepsilon_2$	% of FEA strain
FEA	3,828 $\cdot 10^3$	100,0 %	4,933 $\cdot 10^3$	100,0 %
Matlab Model	3,474 $\cdot 10^3$	90,8 %	4,167 $\cdot 10^3$	84,5 %
FBG Measurement	5,728 $\cdot 10^3$	149,6 %	5,092 $\cdot 10^3$	103,2 %

Table 1: Maximum surface strain values in the Ottobock 1E90 on sensor locations 1 and 2 - calculated by FEA and an inverse MALTAB model, measured by the FBG sensors. Also shown are the percentages of the inverse model and the measured strain compared to the FEA results.

	$\mu\varepsilon_1$	% of FEA strain	$\mu\varepsilon_2$	% of FEA strain
FEA	3,387 $\cdot 10^3$	100,0 %	3,13 $\cdot 10^3$	100,0 %
Matlab Model	3,063 $\cdot 10^3$	91,5 %	2,154 $\cdot 10^3$	67,4 %
FBG Measurement	2,234 $\cdot 10^3$	65,9 %	3,100 $\cdot 10^3$	99,1 %

Table 2: Maximum surface strain values in the ArcX Sport on sensor locations 1 and 2 - calculated by FEA and an inverse MALTAB model, measured by the FBG sensors. Also shown are the percentages of the inverse model and the measured strain compared to the FEA results.

3.2 Variance in system

The static, non-loaded prosthesis tests results are reported in table 3. These results can be interpreted as the variance inherent to the FBG sensing system with data

resampled at 1,98 kHz. Additionally a polarization measurement was done for the ArcX Sport prototype, which reflects the measurement error when perturbing the patch lead of the FBGs. The maximum standard deviation for the unperturbed signal was measured in sensor 4 at $\sigma^2 = 1{,}129\ \mu\varepsilon$, the maximum peak-to-peak value when unperturbed was measured in sensor 3 at 7,681 $\mu\varepsilon$.

When looking at the frequency domain of the signal (see appendix C) some low frequency contributions are present that have larger magnitude than the higher frequency contributions. This is not expected to have large effect on the measurement since the overall variance is low compared to the system output when the sensors are perturbed.

For the polarization, the biggest standard deviation was measured in sensor 4 at $\sigma^2 = 7{,}716\ \mu\varepsilon$, the maximum peak to peak value was measured in sensor 4 at 45,351 $\mu\varepsilon$. Comparing the maximum peak-to-peak values to the maximum measured strains in table 2, the maximal force measurement error due to variance in the FBG measurement system would be ± 3,716 N and the maximal measurement error due to polarization would be ± 21,94 N.

The raw data for these unperturbed signals and the polarization signal can be found in appendix C.

	Unperturbed		Polarization	
	σ^2 [$\mu\varepsilon$]	Peak-to-peak [$\mu\varepsilon$]	σ^2 [$\mu\varepsilon$]	Peak-to-peak [$\mu\varepsilon$]
Sensor 1	0,730	4,309	3,473	27,578
Sensor 2	0,934	6,209	1,849	18,198
Sensor 3	1,059	7,681	5,108	30,508
Sensor 4	1,129	6,781	7,716	45,351
Sensor 5	0,807	4,438	3,781	24,725
Sensor 6	0,475	3,569	2,225	14,697

Table 3: The unperturbed sensor variance and polarization data. Calculated was the standard deviation (σ^2) for both unperturbed signals and the polarization signal, as well as the peak to peak value for both signals.

3.3 Static calibration through compression tests

The calibration curve of the instrumented RSPs was computed using the force measurements in the compression bench (Zwick-Roell 250kN). The result of the calibration of the Gyromotics ArcX Sport can be found in figure 7, the calibration for the Ottobock 1E90 is found in figure 24 in appendix D.

From this data the point of application (l_1 in figure 3) was determined, for the Gyromotics ArcX Sport this is plotted in figure 8 (for Ottobock 1E90 see figure 25 in Appendix D). The observed difference in point of application relative to the initial contact point at maximum displacement was 30 mm for both the Ottobock 1E90 and the Gyromotics ArcX Sport.

The raw data of the compression tests of both the Ottobock 1E90 and the Gyromotics ArcX Sport can be found in appendix D.

The cyclic tests showed 10 N discrepancy after each cycle in the GRF in y-direction, after which the force settled to 0 N after 4 seconds. The GRF in x-direction showed a larger drift of 23 N, which settled to 0 N after 27 seconds.

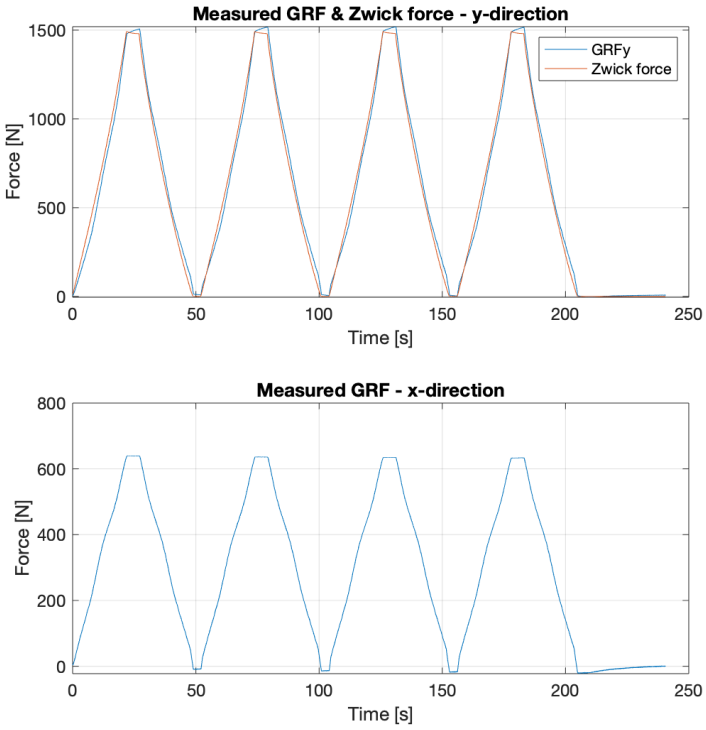

Figure 7: Calibration of GRF for the Gyromotics ArcX Sport. The top graph shows the calibrated GRF in y-direction and Zwick force as reference, the bottom graph shows the corresponding GRF in x-direction. The calibration was performed using an optimization procedure in MATLAB (see section 2.5.1)

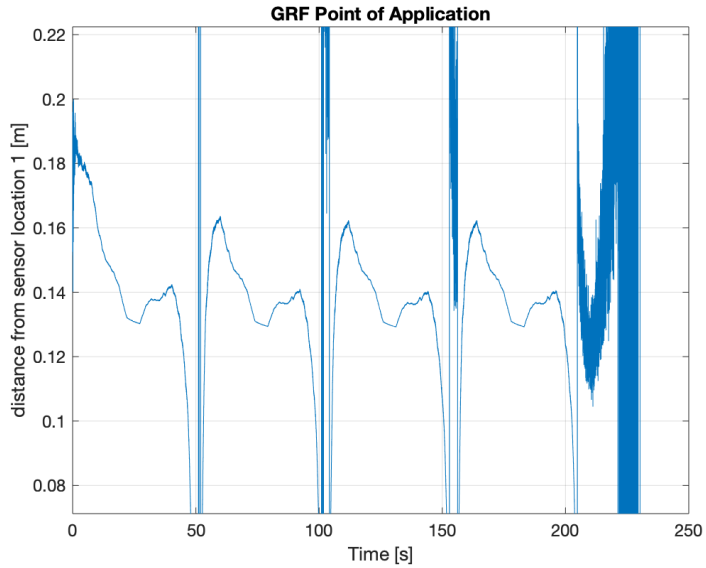

Figure 8: Calculated GRF point of application (l_1 in figure 3). When the GRF is under load, the point of application is approximated well and corresponds to the actual point of contact of the prosthesis (within the range of 0.18 m and 0.13 m). After the load removal the distal end is not in contact with the ground thus the point of application estimation grows to infinity. The change in contact point of contact during compression is estimated at 0,03 m.

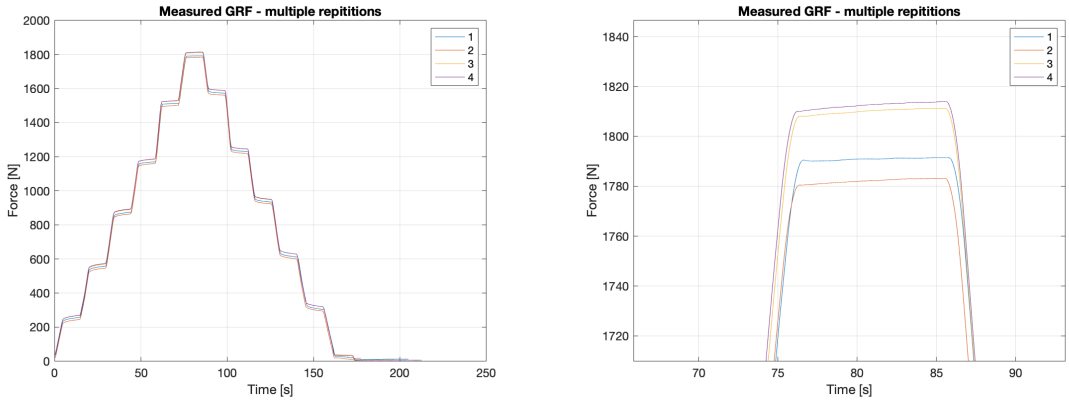

(a) (b)

Figure 9: Computed GRFy based on the FBG data during repeated compression test with the instrumented Gyromotics ArcX Sport. The data is smoothed using a moving mean filter with window of 500 samples. In the 20 compression tests the maximum observed deviation was found to be 29,31 N while a standard deviation of $\sigma^2 = 13.39$ N was found. The variation of the Zwick data had $\sigma^2 = 2.39$ N, and a maximum deviation of 9,43 N was found.

3.3.1 Repeatability

In order to find the accuracy of the sensor system on the Gyromotics ArcX Sport several succeeding compression tests are compared in figure 9a. 20 tests in total, as 5 sets of 4 step tests were performed. The standard deviations of GRFy were found at $\sigma^2 = 13.39$ N, the maximum deviation of the mean GRFy was found to be 29,31 N. The Zwick data variance over the compression tests was also computed. A standard deviation of $\sigma^2 = 2.39$ N was found, and a maximum deviation of 9,43 N was observed.

The measurement error of the FBG computed strains was determined by obtaining the difference between the Zwick force and the GRFy computed through the FBGs. A plot of the measurement error of the trails as shown in figure 9a can be found in figure 10. The root mean squared error of the computed GRFy was 31,46 N over the 20 performed compression tests. The maximum error was found to be 91,3 N. The measured error over the trails was found to be non-normally distributed (see appendix D, figure 27).

3.4 Field tests

In the field tests the strains were recorded over the trails as mentioned in section 2.6. The IMU data was used as input for the orientation RSP relative to the global reference frame. From these strains the GRFs in x-direction and y-direction were computed in a similar manner as in the calibration tests.

The measured GRFs of the first weight shift trail (regular frequency) are reported in figure 11. The peaks in the GRFy indicate the response of the FBGs to the weight shifted over the leg wielding the RSP. The outliers in the data, around the 1.7 second mark, show an effect due to the calibration of the interrogation software, compromising some samples in the data collection.

The measured GRFs for every fourth step of the walking trails are plotted in figure 12. For every variant of the trail (regular step length, short step length and long step length) the average over the three repetitions was taken.

Figure 10: Measurement error of the FBG computed GRFy compared to the Zwick force

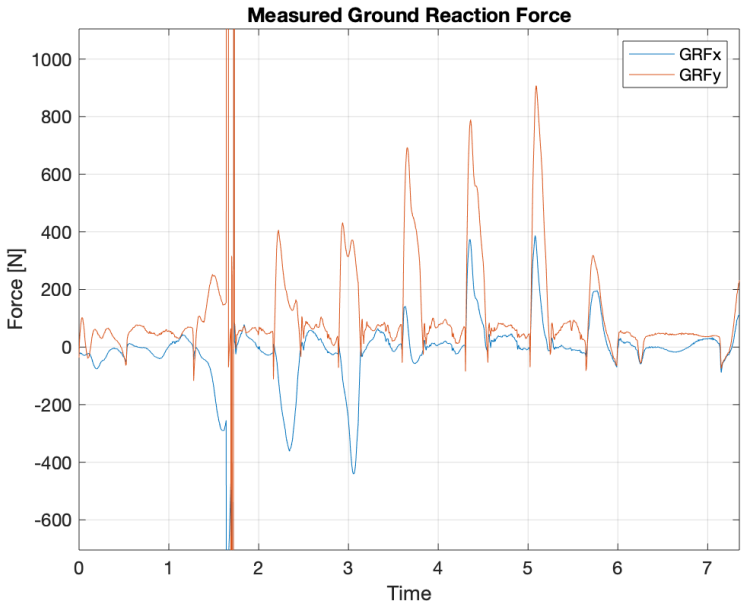

Figure 11: The computed GRF in the first weight shift trail. Both the GRF in x-direction and the GRF in y-directions are plotted. A clear cyclic pattern can be observed in the GRFy and GRFx components.

The short step length (plotted in red) shows a shorter contact time than the long step length and the regular step length. The magnitude of the GRFy was measured lower than the body weight of the participant.

Although the interrogator software calibration was adjusted for the walking trails, a similar interference effect as with the weight shift trail was observed for the first section of the walking trail.

For the higher velocity trails, the data was plotted in a similar way. The fourth step of the single trails was plotted. Per step length variant, the average over the individual trails was taken. These plots can be observed in figures 12.

The field test allowed for the collection of the GRFs over a complete trail. In figure 14 the progression of one single high velocity trail is plotted. It can be observed that the first step has a longer contact time, but the following steps show a similar profile. From these step plots it can be observed that the contact time after the first step increases slightly. The GRFx components have a larger variability The GRF data of the other high velocity trails can be found in appendix E.

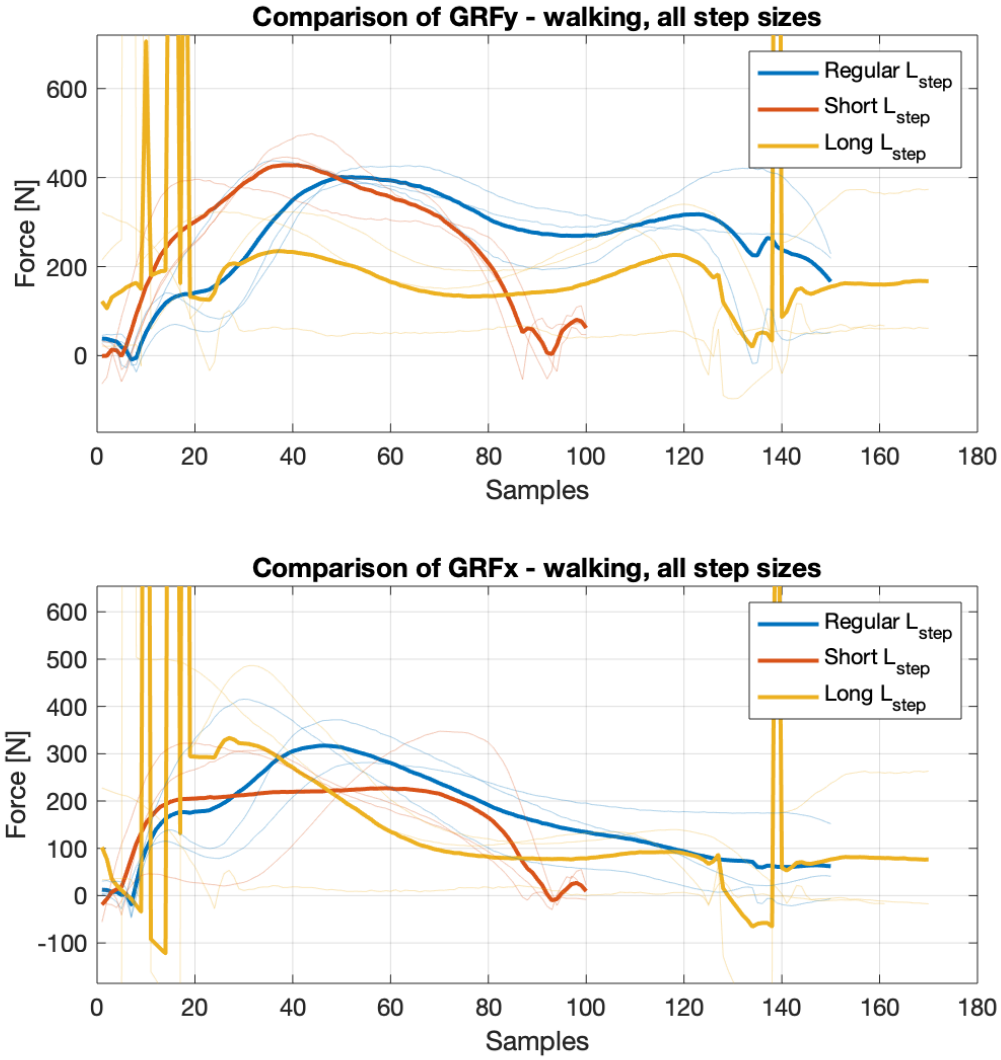

Figure 12: The GRF profiles (GRFy in the top graph, GRFx in the bottom graph) of the field test at walking velocity. Every step was synchronized at the moment of touchdown of the RSP. The thin lines represent every individual fourth step of the trail. The average over the steps per step length (Regular L_{step}, Short L_{step}, Long L_{step}) is plotted in the thicker lines.

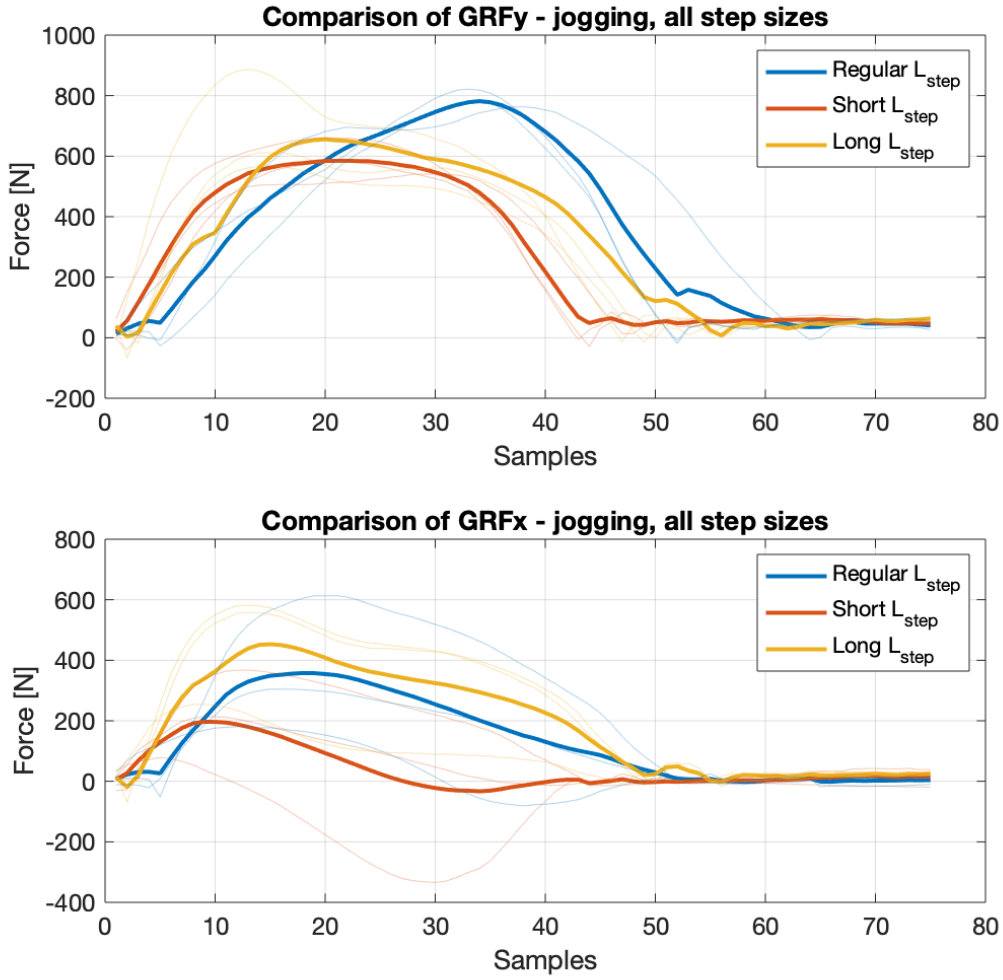

Figure 13: The GRF profiles (GRFy in the top graph, GRFx in the bottom graph) in the running trails. Every step was synchronized at the moment of touchdown of the RSP. The thin lines represent every individual fourth step of the trail. The average over the steps per step length (Regular L_{step}, Short L_{step}, Long L_{step}) is plotted in the thicker lines.

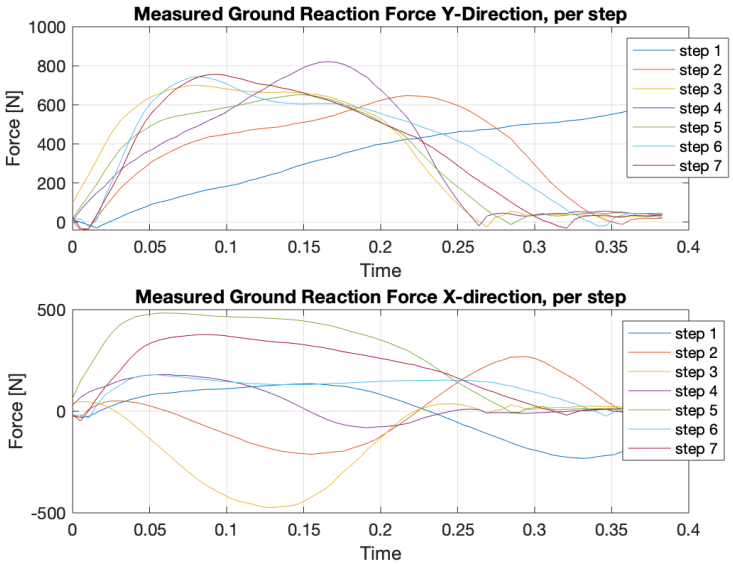

Figure 14: Measured GRF for the regular l_{step} running trial. The single steps are plotted such that at t = 0 RSP has initial contact with the ground. The individual lines represent the steps of the trail. In the GRFy profile all but the first step follow a similar inpulse pattern, with a similar contact time. The GRFx is found less consistent as more variability is shown between individual steps.

4 Discussion

The present study aimed to validate a FOS measurement system in an RSP that could determine the GRF magnitude, direction and its point of application during walking while conforming to the sensor design specifications of section 2.1. This data could allow for validation of newly developed RSP designs or numerically supporting sprinting techniques.

The application of the FBG sensors added no significant weight to the prosthesis. Due to the small sectional area of the optical fibre of the FBGs and the small amounts of adhesive needed to attach the sensors it is unlikely that the mechanical properties of the RSP were altered. No gait impairment was reported by the participant of this study during the field testing.

In terms of the sensing capabilities the FBGs showed a clear response to the perturbations exerted on the RSP. This was shown in the results of the field tests, where the cyclic impulse from touchdown of the RSP can be observed clearly in the resultant GRF measurements. No FBG interference occurred during the compression testing or the field testing.

Measurements errors from external sources like temperature strain (approximately 10 $\mu\varepsilon/^{\circ}$C [5]), have a negligible effect on the FBG variance/bias since low change in environmental temperature change is expected and the mechanical strain components due to high forces are relatively large.

The variance in the sensor system could be lowered when averaging the signal, at cost of lower Sampling frequency (f_s). Taking into account the contact time of the user of the RSP, a sufficient high f_s is needed for good analysis throughout a step, so care must be taken when averaging the data. The used equipment has that headroom, and is therefore suitable for further analysis of the measurement system.

The results of the tests in section 3.2 and section 3.3 have shown that in the

case of the GRFy component, the sensor system specifications comply to the sensor design requirements stated in 2.1. Adding up the maximal variance and precision errors, the maximal measurement error is below the stated 5 % of the 3.24 times bodyweight (for a person of 70kg).

Sampling frequency		1,928 kHz
Precision	Variance	3,716 N
	Polarization	21,94 N
Accuracy (max deviation observed)		91,6 N
Resolution		0,209 $\mu\varepsilon$
Linearized Sensitivity		0,121 N/$\mu\varepsilon$
Response time		0,08 s

Table 4: The calculated sensor system specifications are retrieved from the static tests and compression bench tests at the given sampling frequency.

In the field test it was shown that the measured GRFy component was a factor 2 lower than expected for the running trails; for similar running speeds, a GRFy was reported of more than 2 times body weight[6, 4]. Although the magnitude difference is apparent, the profile of the response showed to be similar to previously measured GRF profiles in y-direction. The magnitude difference can be explained by the calibration method, which utilizes only a 1-DOF force measurement (in y-direction), and lacks the capability of capturing forces in x-direction and moments appearing in the fixture of the RSP.

The main limitation of the adopted approach is that the estimation of the GRF in x-direction is likely flawed. The variability in the GRFx component in the field tests showed to be of a large magnitude, and showed no repeated behaviour like the y-component of the GRF. No such variability in the GRFx component has been shown in literature[1, 4, 8], so further analysis of the horizontal force collection by the instrumented RSP is needed.

The variability measured in the field tests can be partially explained by the variance in steps of the participant. Also the lack of a calibration in the x-direction could explain the variance of the GRFx component. Additional measurements with force plates needs to be performed to further validate the findings, and a calibration method in which the force in x-direction can be determined is needed.

For this prototype the sensors were attached to the RSP surface. In order for the sensor system to work in a sprint training environment, it is recommended to embed the optical fibre that the FBGs are written in into the CFRP laminate. This would reduce the fragility of the system while not impairing the measurement capabilities of the system as seen in the research by Galvao et al. [2]. Additionally an ambulant interrogation system needs to be utilized so that the athlete is not constraint in its movement.

5 Conclusions

- The proposed sensor system complies to the set of practical requirements stated in section 2.1.
- For the y-component of the GRF, the proposed sensing method complies with the set requirements in section 2.1.
- The magnitude of the GRFy component in the field tests showed to be a factor 2 lower than expected when compared to findings in literature [6, 4], while the calibrated force in the compression testing didn't show such discrepancies.
- The x-component of the GRF showed to have a high variability in the field tests, and therefore additional research needed in this aspect.
- The point of application of the GRF could be determined for both prostheses.
- The spectral design for both the Ottobock 1E90 and the Gyromotics ArcX Sportblade showed to work well in the chosen applications, as no sensor interference occurred during the compression testing and the field testing.
- Additional work needs to be done in calibration of the FBG measurement system using a calibration bench with more than 1 DOF in order to measure the moments and forces in x-direction of the RSP.

References

[1] Gert-Peter Brüggemann, Adamantios Arampatzis, Frank Emrich, and Wolfgang Potthast. Biomechanics of double transtibial amputee sprinting using dedicated sprinting prostheses. *Sports Technology*, 1(4):220–227, 2008.

[2] J.R. Galvão, C.R. Zamarreño, C. Martelli, J.C. Cardozo Da Silva, F.J. Arregui, and I.R. Matías. Smart Carbon Fiber Transtibial Prosthesis Based on Embedded Fiber Bragg Gratings. *IEEE Sensors Journal*, 18(4):1520–1527, 2018.

[3] Hiroaki Hobara, Yoshiyuki Kobayashi, Thijs A Heldoorn, and Masaaki Mochimaru. The fastest sprinter in 2068 has an artificial limb? *Prosthetics and Orthotics International*, 39(6), 2014.

[4] Nicola Petrone, Gianfabio Costa, Gianmario Foscan, Antonio Gri, Rosanne Boekestijn, Gianluca Migliore, and Andrea Cutti. Collection of Structural Loads Acting on Instrumented Running Specific Prostheses during Field Tests on Elite Atletes. *Proceedings*, 49:74, 6 2020.

[5] Manjusha Ramakrishnan, Ginu Rajan, Yuliya Semenova, and Gerald Farrell. Overview of fiber optic sensor technologies for strain/temperature sensing applications in composite materials. *Sensors (Switzerland)*, 16(1), 2016.

[6] Peter G Weyand, Matthew W Bundle, Craig P McGowan, Alena M Grabowski, Mary Beth Brown, Rodger Kram, and Hugh Herr. The fastest runner on artificial legs: different limbs, similar function? *Journal of Applied Physiology*, 107(3):903–911, 2009.

[7] Peter G Weyand, Rosalind F Sandell, Danille N L Prime, and Matthew W Bundle. The biological limits to running speed are imposed from the ground up. *Journal of Applied Physiology*, 108(4):950–961, 2010.

[8] Peter G Weyand, Deborah B Sternlight, Matthew J Bellizzi, and Seth Wright. Faster top running speeds are achieved with greater ground forces not more rapid leg movements. *Journal of Applied Physiology*, 89(5):1991–1999, 2000.

A Appendix A - Spectral design, sensor layout

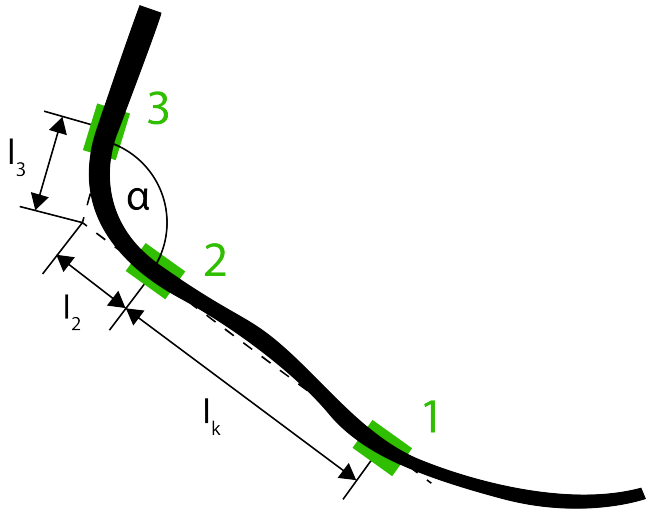

Figure 15: Sensor Locations on the Gyromotics ArcX Sport. The sensors are placed on the top and bottom of the locations 1, 2, and 3 creating a so-called sensor bridge.

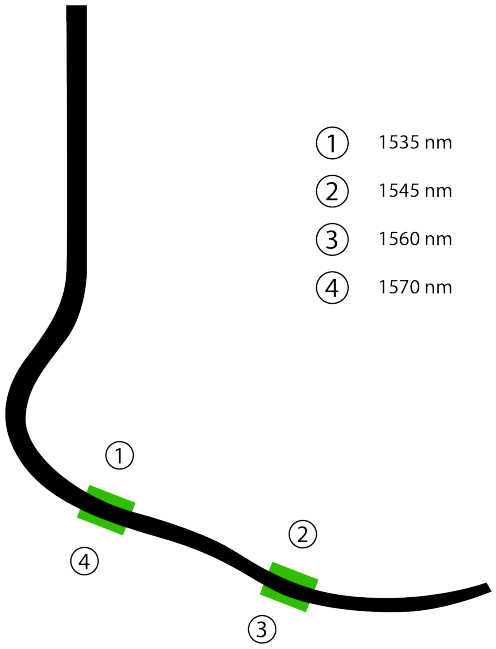

Figure 16: Sensor layout instrumented Ottobock 1E90

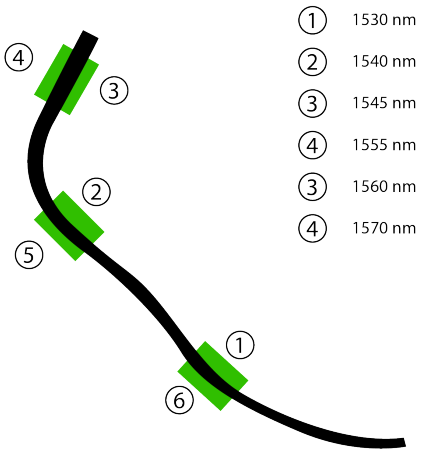

Figure 17: Sensor layout instrumented Gyromotics ArcX Sport

B Appendix B - FEA results

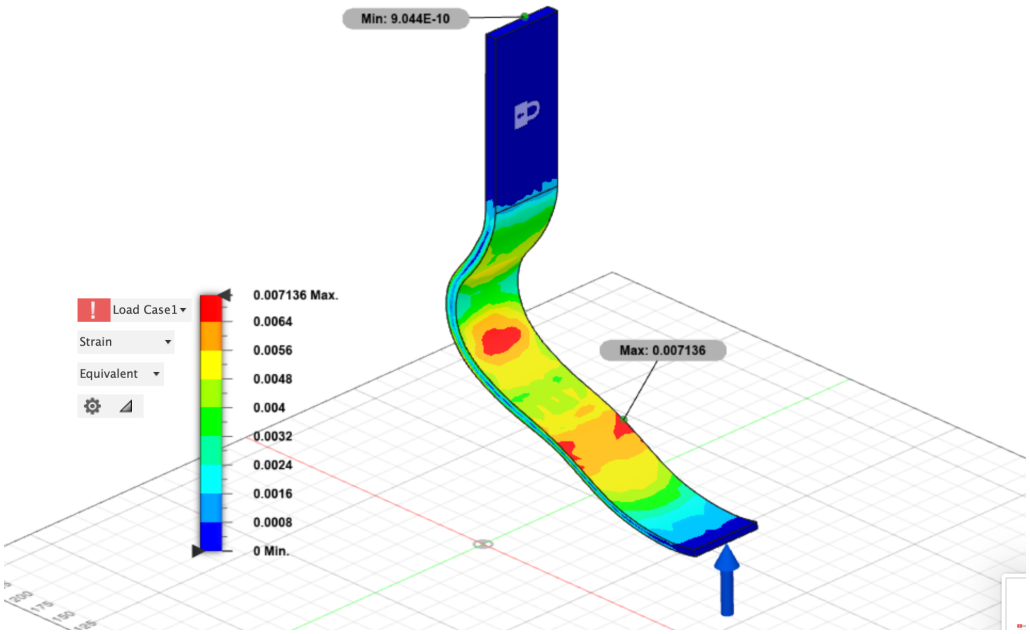

Figure 18: FEA results Ottobock 1E90

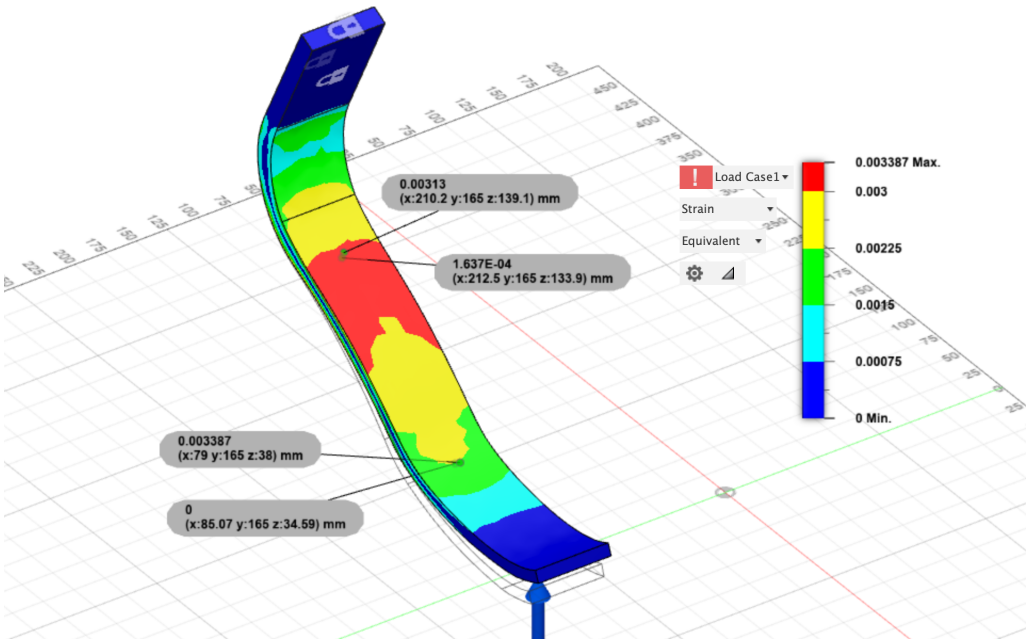

Figure 19: FEA results Gyromotics ArcX Sport

C Appendix C - Raw Polarization data

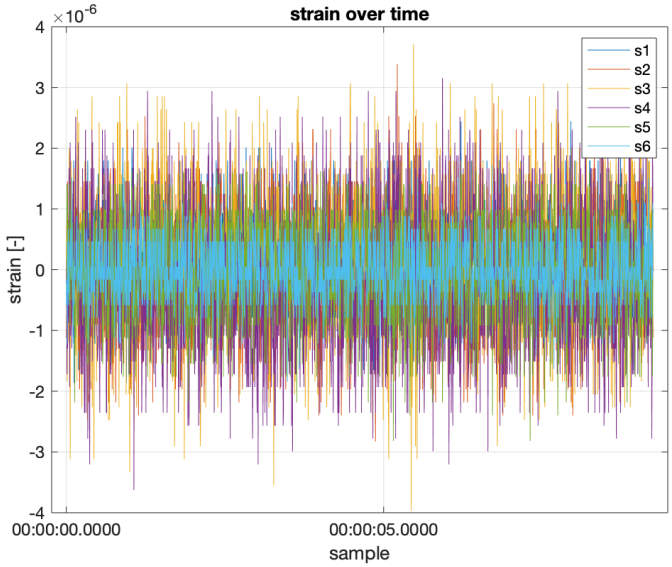

Figure 20: Raw unperturbed FBG data (Gyromotics ArcX Sport).

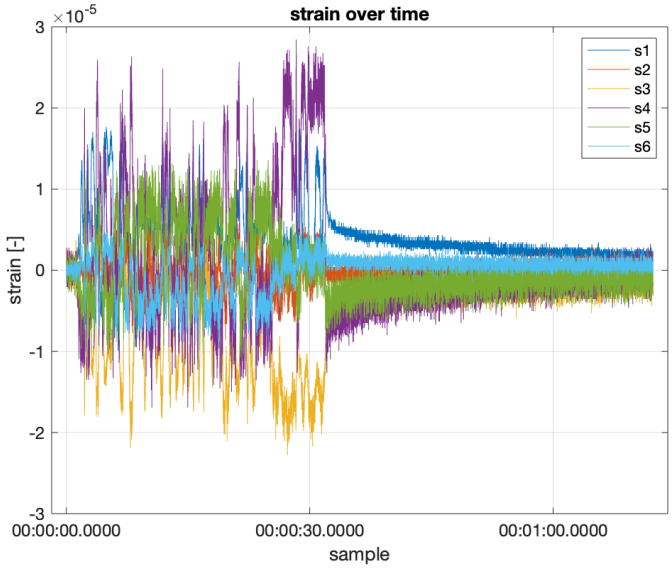

Figure 21: Raw Polarization FBG data (Gyromotics ArcX Sport).

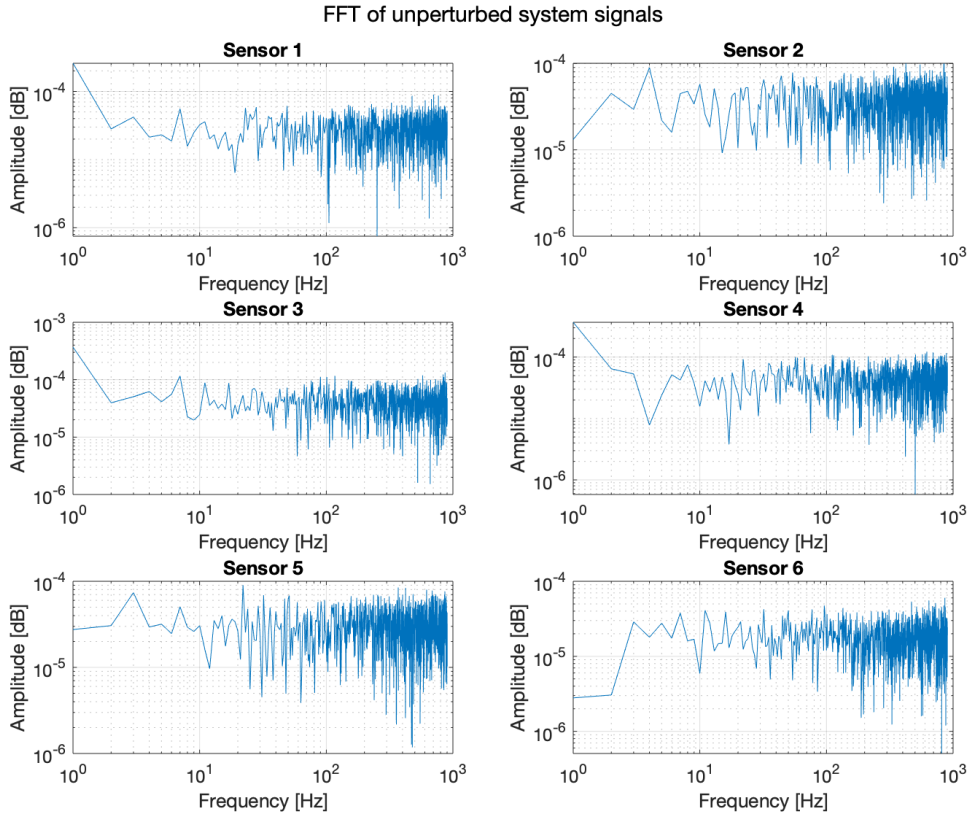

Figure 22: FFT of raw, unperturbed FBG data (Gyromotics ArcX Sport). It can be observed that in sensor 1, sensor 3 and sensor 4 there is some higher magnitude low-frequency contribution present in the signals. The other signals resemble a white noise signal.

D Appendix D - Raw compression test data

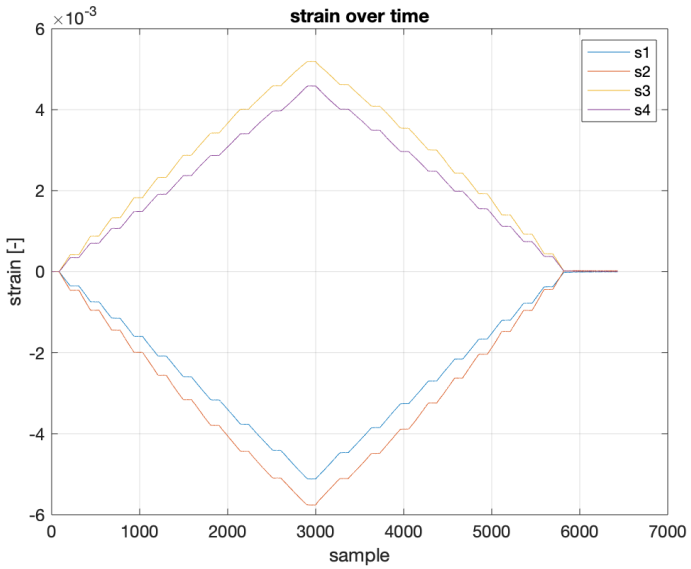

Figure 23: Raw strain data as measured during the compression testing in the Ottobock 1E90. Sensor numbers corresponding to the strains can be found in the Method section.

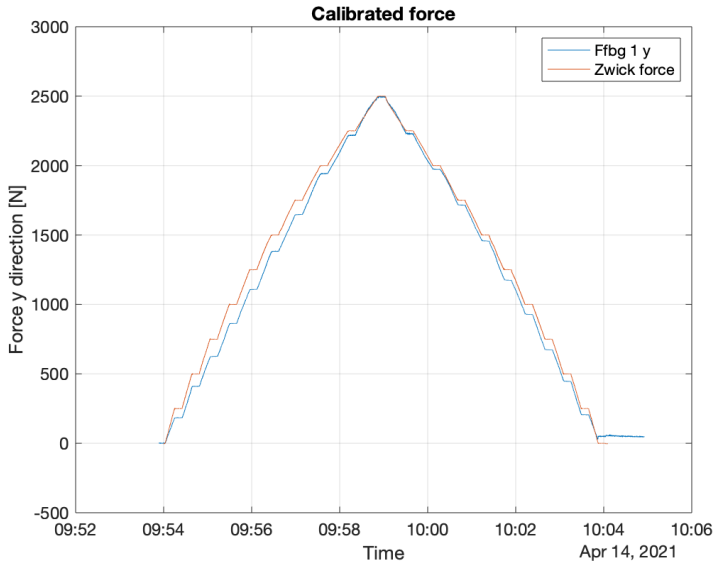

Figure 24: Calibrated y-force curve of the Ottobock 1E90. Zwick force is the measured force in the compression bench, GRFy is the computed force in y-direction calculated from the measured strains in the RSP. The calibration for the 1E90 was done by scaling the maximum calculated force with the measured force in the Zwick (scaling factor C = 0.8600).

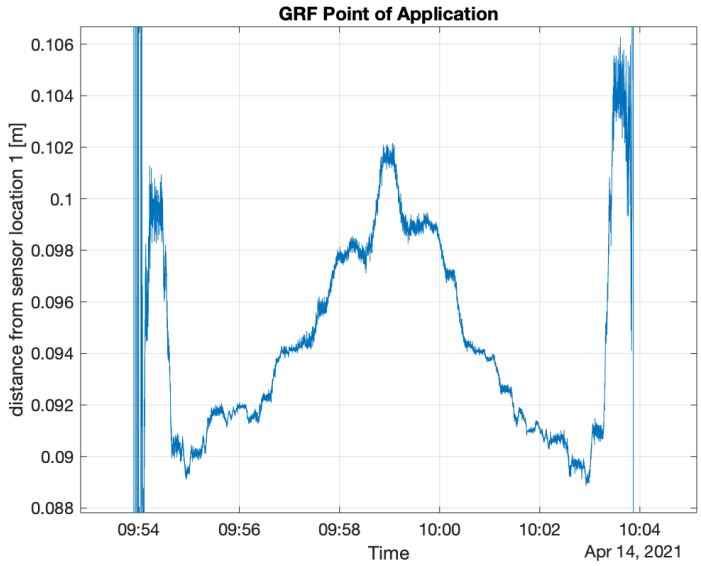

Figure 25: GRF Point of application in the Ottobock 1E90 compression test.

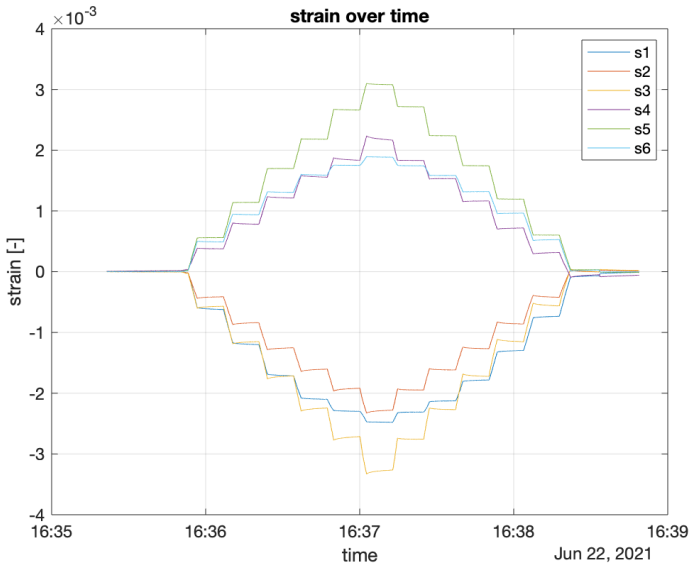

Figure 26: Raw strain data as measured during the compression testing in the ArcX Sport. Sensor numbers corresponding to the strains can be found in the Method section.

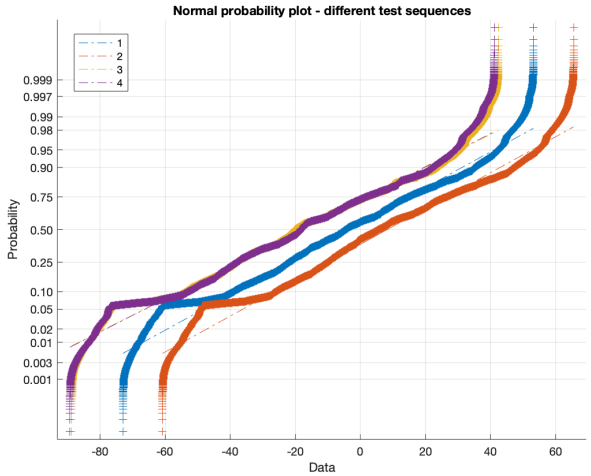

Figure 27: Normal probability plot for the measured error (difference in Zwick force and GRFy computed through FBG sensors) in several compression tests. These plots indicate that the used calibration method

E Appendix E - Raw field test data

E.1 Jogging trails - short l_{step}

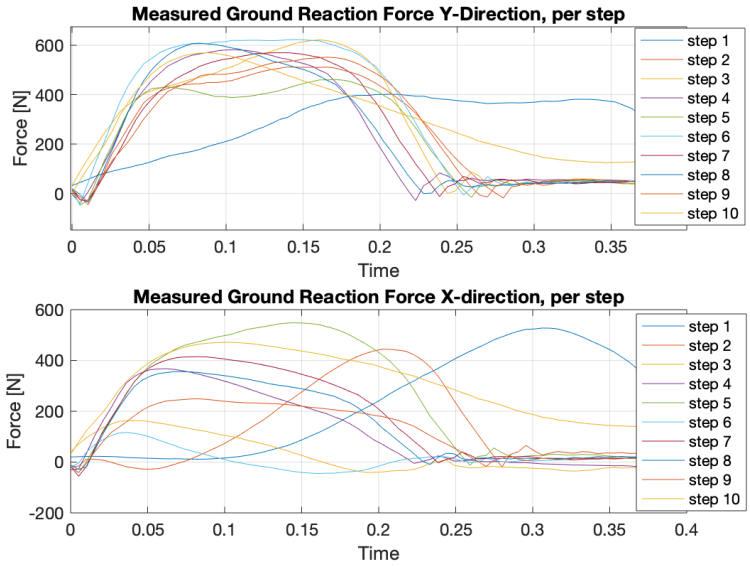

Figure 28: Jogging short l_{step} - trail 1. Individual lines represent the steps of the entire trail.

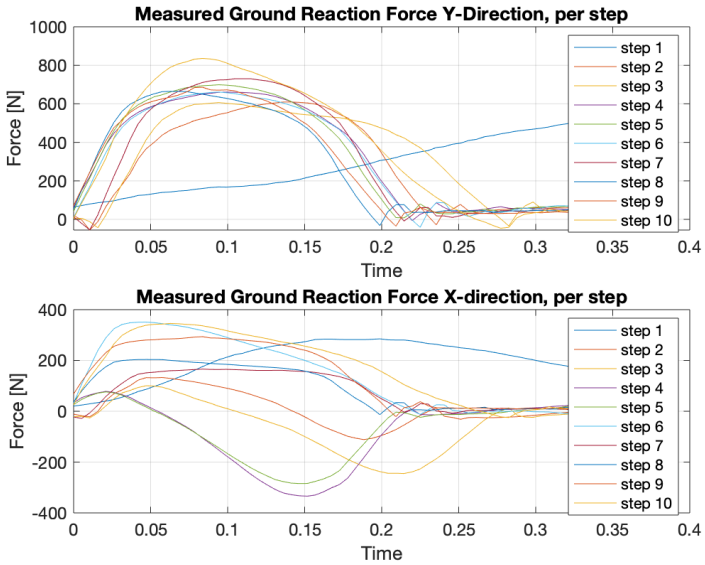

Figure 29: Jogging short l_{step} - trail 2. Individual lines represent the steps of the entire trail.

E.2 Jogging trails - regular l_{step}

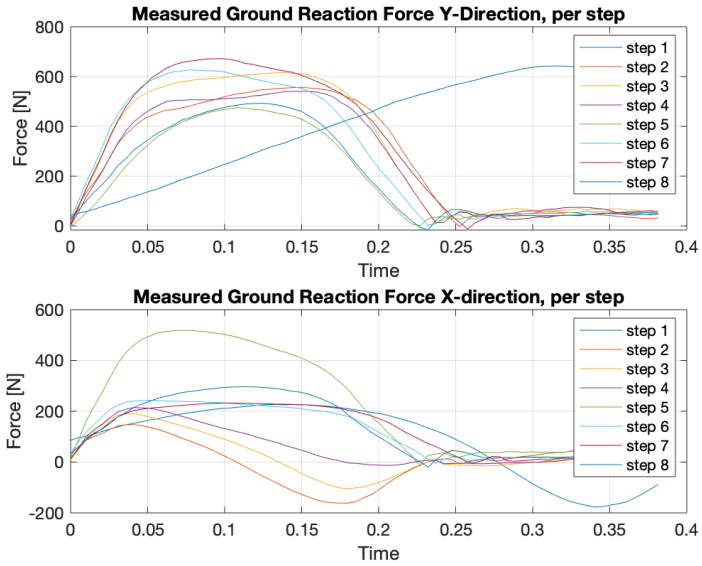

Figure 30: Jogging short l_{step} - trail 3. Individual lines represent the steps of the entire trail.

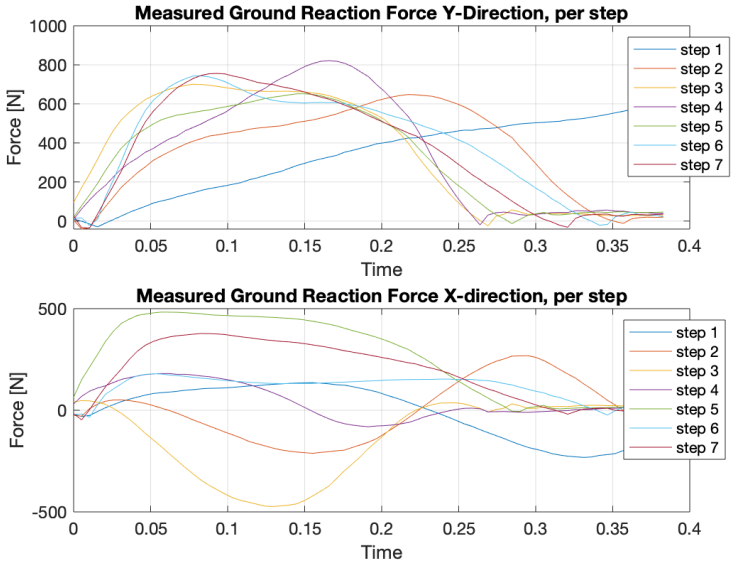

Figure 31: Jogging regular l_{step} - trail 1. Individual lines represent the steps of the entire trail.

E.3 Jogging trails - long l_{step}

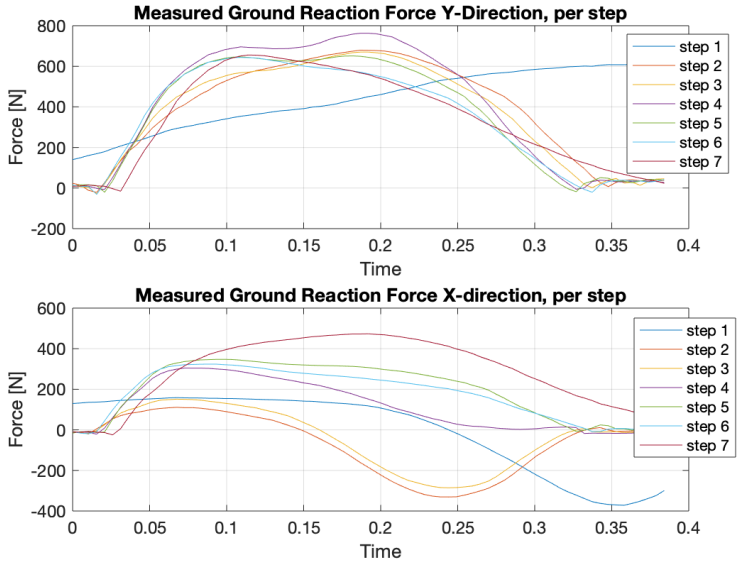

Figure 32: Jogging regular l_{step} - trail 2. Individual lines represent the steps of the entire trail.

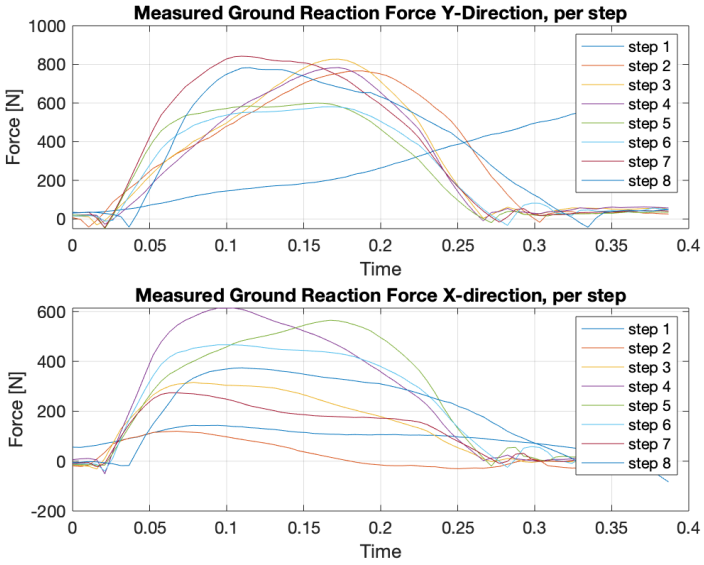

Figure 33: Jogging regular l_{step} - trail 3. Individual lines represent the steps of the entire trail.

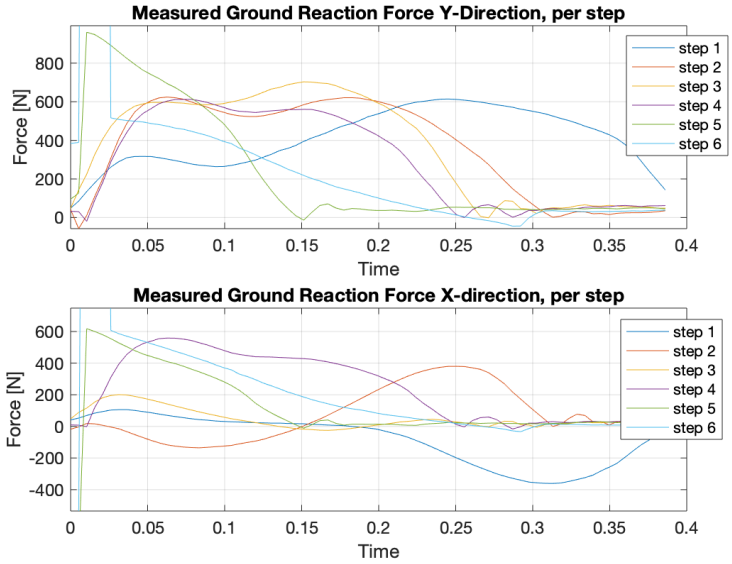

Figure 34: Jogging long l_{step} - trail 1. Individual lines represent the steps of the entire trail.

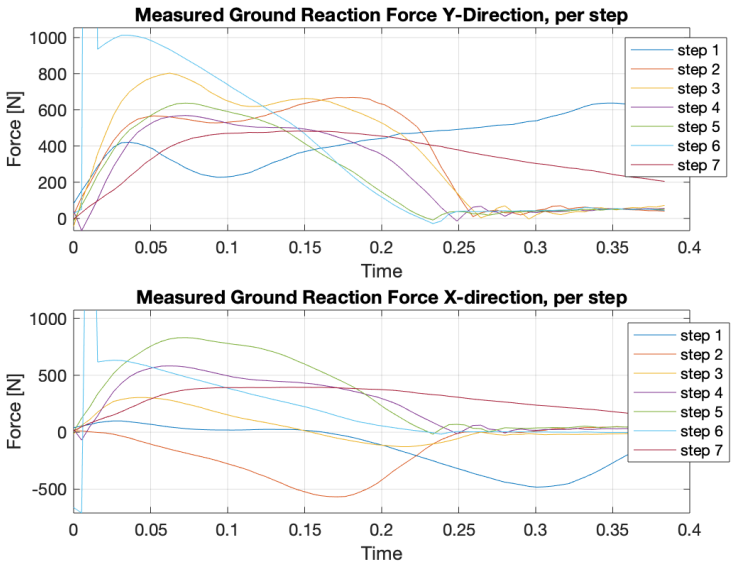

Figure 35: Jogging long l_{step} - trail 2. Individual lines represent the steps of the entire trail.

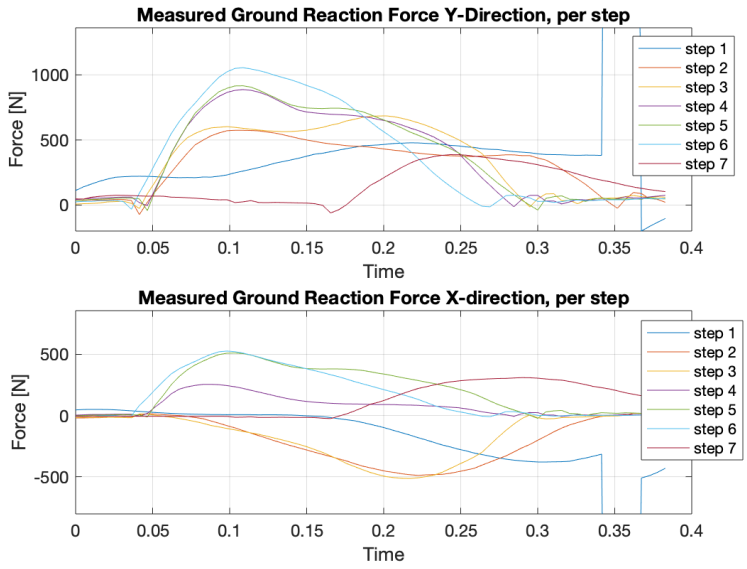

Figure 36: Jogging long l_{step} - trail 3. Individual lines represent the steps of the entire trail.

F Appendix F - Inverse calculation model

```
clear all
close all
clc


%% Constants
%
   %-----------------------------------------------------------------


numsens = 2;

% material properties
E   = 140e+9;           % AS4/3501-6 Carbon/Epoxy laminate
LCS = 1.725e+9;         % compressive strength cfrp

% % ArcX sport
% b = 0.059;                    % width prosthesis
% h = [0.0095 0.0123];          % height prosthesis
   perpendicular to arm
% y = [0.00945 0.0123]*0.5;     % Distance from midline
% lk = 0.17;                          % distance between
    FBG locations

% Ottobock 1E90
b = 0.070;                           % width prosthesis
% h = [0.00945 0.0065];               % height prosthesis
    perpendicular to arm
% y = [0.00945 0.0065]*0.5;           % Distance from
   midline

h = [0.0065 0.00945];                % height prosthesis
   perpendicular to arm
y = [0.0065 0.00945]*0.5;            % Distance from
   midline


lk = 0.155;                          % distance between
   FBG locations

l1 = 0.1;                            % Estimated dist to
   contact point

A = h.*b;                            % section area
I = b*h.^3/12;                       % Inertia

```

```
37
38
39  %% GRF signal generation
40
41  fs = 1000;
42
43  GRFy_max = 2500;
44  GRFx_max = 500;
45
46  t = linspace(0,1-1/fs,fs);
47
48  GRFy = GRFy_max*sin(t*pi);
49  GRFx = -GRFx_max*sin(t*2*pi);
50
51
52  %% Rotate to local reference frame
53
54  beta = linspace(5,20,(fs)/2);
55  beta = [beta flip(beta)];
56  beta = deg2rad(beta);
57
58  GRF = [GRFx; GRFy];
59
60  F = zeros(2,fs);
61
62  for i = 1:length(GRF(1,:))
63
64      angle = beta(i);
65
66      Rlg =  [ cos(angle)  sin(angle);
67              -sin(angle)  cos(angle)];
68
69      F(:,i) = Rlg\GRF(:,i);
70  end
71
72  %%
73
74  Fa = -F(1,:);
75  Fb = -F(2,:);
76
77  M1 = Fb.*l1;
78  M2 = Fb*lk+M1;
79
80
81  %% Determining strains
82
83  sigma_a = zeros(fs,numsens);
84  s_a     = zeros(fs,numsens);
```

```
85
86  for i = 1:numsens
87      sigma_a(:,i) = Fa./A(i);
88      s_a(:,i)     = sigma_a(:,i)./LCS;
89  end
90
91
92  s_b(:,1) = -M1*y(1)/(I(1)*E);
93  s_b(:,2) = -M2*y(2)/(I(2)*E);
94
95
96  s(:,1) = s_b(:,1) + s_a(:,1);
97  s(:,4) = -s(:,1);
98
99
100 s(:,2) = s_b(:,2) + s_a(:,2);
101 s(:,3) = -s(:,2);
102
103 %% Plotting
104
105 figure()
106 plot(t,GRFy); hold on
107 plot(t,GRFx)
108 grid on
109 xlabel('time')
110 ylabel('Force [N]')
111 legend('GRFy','GRFx')
112 title('Ground Reaction Force over time')
113
114 figure()
115 plot(t,s);
116 grid on
117 xlabel('time')
118 ylabel('strain [-]')
119 legend('s1','s2','s3','s4')
120 title('strain over time')
121
122 figure()
123 plot(t,s_a)
124 grid on
125 xlabel('time')
126 ylabel('strain, axial portion [-]')
127 legend('bridge 1','bridge 2')
128 title('axial strain over time')
129
130 figure()
131 plot(t,s_b)
132 grid on
```

```
133 xlabel('time')
134 ylabel('strain, bending portion [-]')
135 legend('bridge 1','bridge 2')
136 title('bending strain over time')
```

G Appendix G

```
clear all
close all
clc


%% Constants
%
   %-----------------------------------------------------------------


numsens = 2;

% material properties
E   = 140e+9;           % AS4/3501-6 Carbon/Epoxy laminate
LCS = 1.725e+9;         % compressive strength cfrp

% % ArcX sport
% b = 0.059;                    % width prosthesis
% h = [0.0095 0.0123];          % height prosthesis
   perpendicular to arm
% y = [0.00945 0.0123]*0.5;     % Distance from midline
% lk = 0.17;                          % distance between
    FBG locations

% Ottobock 1E90
b = 0.070;                           % width prosthesis
% h = [0.00945 0.0065];               % height prosthesis
    perpendicular to arm
% y = [0.00945 0.0065]*0.5;           % Distance from
   midline

h = [0.0065 0.00945];                % height prosthesis
   perpendicular to arm
y = [0.0065 0.00945]*0.5;            % Distance from
   midline


lk = 0.155;                          % distance between
   FBG locations

l1 = 0.1;                            % Estimated dist to
   contact point

A = h.*b;                            % section area
I = b*h.^3/12;                       % Inertia

```

```
37
38
39  %% GRF signal generation
40
41  fs = 1000;
42
43  GRFy_max = 2500;
44  GRFx_max = 500;
45
46  t = linspace(0,1-1/fs,fs);
47
48  GRFy = GRFy_max*sin(t*pi);
49  GRFx = -GRFx_max*sin(t*2*pi);
50
51
52  %% Rotate to local reference frame
53
54  beta = linspace(5,20,(fs)/2);
55  beta = [beta flip(beta)];
56  beta = deg2rad(beta);
57
58  GRF = [GRFx; GRFy];
59
60  F = zeros(2,fs);
61
62  for i = 1:length(GRF(1,:))
63
64      angle = beta(i);
65
66      Rlg =  [ cos(angle)  sin(angle);
67              -sin(angle)  cos(angle)];
68
69      F(:,i) = Rlg\GRF(:,i);
70  end
71
72  %%
73
74  Fa = -F(1,:);
75  Fb = -F(2,:);
76
77  M1 = Fb.*l1;
78  M2 = Fb*lk+M1;
79
80
81  %% Determining strains
82
83  sigma_a = zeros(fs,numsens);
84  s_a     = zeros(fs,numsens);
```

```
85
86  for i = 1:numsens
87      sigma_a(:,i) = Fa./A(i);
88      s_a(:,i)     = sigma_a(:,i)./LCS;
89  end
90
91
92  s_b(:,1) = -M1*y(1)/(I(1)*E);
93  s_b(:,2) = -M2*y(2)/(I(2)*E);
94
95
96  s(:,1) = s_b(:,1) + s_a(:,1);
97  s(:,4) = -s(:,1);
98
99
100 s(:,2) = s_b(:,2) + s_a(:,2);
101 s(:,3) = -s(:,2);
102
103 %% Plotting
104
105 figure()
106 plot(t,GRFy); hold on
107 plot(t,GRFx)
108 grid on
109 xlabel('time')
110 ylabel('Force [N]')
111 legend('GRFy','GRFx')
112 title('Ground Reaction Force over time')
113
114 figure()
115 plot(t,s);
116 grid on
117 xlabel('time')
118 ylabel('strain [-]')
119 legend('s1','s2','s3','s4')
120 title('strain over time')
121
122 figure()
123 plot(t,s_a)
124 grid on
125 xlabel('time')
126 ylabel('strain, axial portion [-]')
127 legend('bridge 1','bridge 2')
128 title('axial strain over time')
129
130 figure()
131 plot(t,s_b)
132 grid on
```

```
133 xlabel('time')
134 ylabel('strain, bending portion [-]')
135 legend('bridge 1','bridge 2')
136 title('bending strain over time')
```

H Appendix G

```
clear all
close all
clc


%% Constants
%
   %-------------------------------------------------------------------------


numsens = 2;

% material properties
E   = 140e+9;           % AS4/3501-6 Carbon/Epoxy laminate
LCS = 1.725e+9;         % compressive strength cfrp

% % ArcX sport
% b = 0.059;                    % width prosthesis
% h = [0.0095 0.0123];          % height prosthesis
   perpendicular to arm
% y = [0.00945 0.0123]*0.5;     % Distance from midline
% lk = 0.17;                          % distance between
    FBG locations

% Ottobock 1E90
b = 0.070;                           % width prosthesis
% h = [0.00945 0.0065];               % height prosthesis
    perpendicular to arm
% y = [0.00945 0.0065]*0.5;           % Distance from
   midline

h = [0.0065 0.00945];                % height prosthesis
   perpendicular to arm
y = [0.0065 0.00945]*0.5;            % Distance from
   midline


lk = 0.155;                          % distance between
   FBG locations

l1 = 0.1;                            % Estimated dist to
   contact point

A = h.*b;                            % section area
I = b*h.^3/12;                       % Inertia

```

```
37
38
39  %% GRF signal generation
40
41  fs = 1000;
42
43  GRFy_max = 2500;
44  GRFx_max = 500;
45
46  t = linspace(0,1-1/fs,fs);
47
48  GRFy = GRFy_max*sin(t*pi);
49  GRFx = -GRFx_max*sin(t*2*pi);
50
51
52  %% Rotate to local reference frame
53
54  beta = linspace(5,20,(fs)/2);
55  beta = [beta flip(beta)];
56  beta = deg2rad(beta);
57
58  GRF = [GRFx; GRFy];
59
60  F = zeros(2,fs);
61
62  for i = 1:length(GRF(1,:))
63
64      angle = beta(i);
65
66      Rlg =  [ cos(angle)  sin(angle);
67              -sin(angle)  cos(angle)];
68
69      F(:,i) = Rlg\GRF(:,i);
70  end
71
72  %%
73
74  Fa = -F(1,:);
75  Fb = -F(2,:);
76
77  M1 = Fb.*l1;
78  M2 = Fb*lk+M1;
79
80
81  %% Determining strains
82
83  sigma_a = zeros(fs,numsens);
84  s_a     = zeros(fs,numsens);
```

```
85
86  for i = 1:numsens
87      sigma_a(:,i) = Fa./A(i);
88      s_a(:,i)     = sigma_a(:,i)./LCS;
89  end
90
91
92  s_b(:,1) = -M1*y(1)/(I(1)*E);
93  s_b(:,2) = -M2*y(2)/(I(2)*E);
94
95
96  s(:,1) = s_b(:,1) + s_a(:,1);
97  s(:,4) = -s(:,1);
98
99
100 s(:,2) = s_b(:,2) + s_a(:,2);
101 s(:,3) = -s(:,2);
102
103 %% Plotting
104
105 figure()
106 plot(t,GRFy); hold on
107 plot(t,GRFx)
108 grid on
109 xlabel('time')
110 ylabel('Force [N]')
111 legend('GRFy','GRFx')
112 title('Ground Reaction Force over time')
113
114 figure()
115 plot(t,s);
116 grid on
117 xlabel('time')
118 ylabel('strain [-]')
119 legend('s1','s2','s3','s4')
120 title('strain over time')
121
122 figure()
123 plot(t,s_a)
124 grid on
125 xlabel('time')
126 ylabel('strain, axial portion [-]')
127 legend('bridge 1','bridge 2')
128 title('axial strain over time')
129
130 figure()
131 plot(t,s_b)
132 grid on
```

```
133 xlabel('time')
134 ylabel('strain, bending portion [-]')
135 legend('bridge 1','bridge 2')
136 title('bending strain over time')
```